Journal of Hazardous Materials 173 (2010) 474–479

Contents lists available at ScienceDirect

Journal of Hazardous Materials

journal homepage: www.elsevier.com/locate/jhazmat

Degradation characteristics of humic acid over iron oxides/Fe^0 core–shell nanoparticles with UVA/H_2O_2

Yulun Nie, Chun Hu*, Lei Zhou, Jiuhui Qu, Qunshan Wei, Dongsheng Wang

State Key Laboratory of Environmental Aquatic Chemistry, Research Center for Eco-Environmental Sciences, Chinese Academy of Sciences, Beijing 100085, China

ARTICLE INFO

Article history:
Received 15 April 2009
Received in revised form 25 August 2009
Accepted 25 August 2009
Available online 31 August 2009

Keywords:
Humic acid
DBP
Fenton
Iron
Electron transfer
Galvanic cells

ABSTRACT

Iron oxides coated on Fe^0 core–shell nanospheres (nIOCI) were synthesized through the reduction of ferrous sulfate aqueous solution by sodium borohydride at ambient atmosphere. The catalyst was highly effective for the degradation of humic acid (HA) in the presence of H_2O_2 and UVA at neutral pH. Under deoxygenated conditions in the dark, the generation of hydroxyl radicals in aqueous nIOCI dispersion verified its galvanic cell-like performance, which enhanced the interfacial electron transfer and led to its higher reactivity. By the total organic carbon, the absorbance of UV_{254}, FTIR, the molecular weight distribution and the chemical fractional character analysis, the degradation process of HA was shown to proceed by the disappearance of aromaticity, the increase of hydrophilic fraction and aromatic ring openings into CO_2 and small organic acid. The treated HA showed much lower reactivity toward chlorine and the disinfection byproduct (DBP) formation potential was also greatly reduced. Moreover, it was found that the DBP formation potential more depended on the structure of the intermediates of HA degradation than TOC removal.

1. Introduction

Humic acids (HA) are among the most widely natural organic matter (NOM) present in virtually all drinking water sources and pose a variety of problems in treatment operations and distribution systems [1]. These substances have been reported to affect the appearance and taste of the water [2]. Moreover, they could react with chlorine via a combination of substitution and oxidation mechanisms [3] to form potentially carcinogenic organic compounds [4] when water was treated with chlorine for sterilization, and this has become a problem in drinking water treatment.

Besides the traditional treatments of humic acids [5–8], studies of the degradation of HA have been carried out with advanced oxidation processes (AOPs) [9–13], among which the heterogeneous Fenton system has attracted great attention due to its formation of highly potent chemical species, •OH, for non-selective oxidation [14,15]. Zero valent iron has been widely used in different environmental treatment processes [16,17] and the direct electron transfer from Fe^0 to H_2O_2 during a Fenton reaction is a very slow process at neutral pH [18]. However, Fe^0/Fe_3O_4 composite showed highly catalytic activity for the decomposition of H_2O_2 as a result of an electron transfer process from metal to magnetite [18,19].

In this paper, nIOCI nanoparticles were synthesized by the reaction between ferrous sulfate and sodium borohydride at ambient atmosphere. It has been reported that the existence of humic acid greatly extended the optimum pH range of the Fenton process toward neutral pH [20], since many types of wastewater usually have pH higher than 4. Herein humic acid was used to assess the performance of the nIOCI/H_2O_2/UVA system at neutral pH. The relationship of the structural characteristics of degraded HA and the DBP formation was proposed on the basis of different experimental information. These results indicated that the destruction of the aromaticity of HA was more important than the removal of TOC from HA for the control of DBP.

2. Experimental

2.1. Materials and reagents

Unless noted otherwise, all reagents used in this work were analytical grade and were used without further purification. Humic acid and Fast Blue BB salt were purchased from Sigma–Aldrich Co. Ferrous sulfate heptahydrate, sodium borohydride, H_2O_2 (30%, w/w) and dimethyl sulfoxide were obtained from Yili Company. All solutions were prepared with deionized and doubly distilled water and the solution pH was adjusted by a diluted aqueous solution of NaOH or HCl.

* Corresponding author. Tel.: +86 10 62849628; fax: +86 10 62923541.
E-mail addresses: nyl@sdu.edu.cn, huchun@rcees.ac.cn (C. Hu).

0304-3894/$ – see front matter.
doi:10.1016/j.jhazmat.2009.08.109

2.2. Catalysts synthesis

The nIOCl nanoparticles were synthesized by the reaction between ferrous sulfate and sodium borohydride in a 250-mL three-necked round-bottle flask. In a typical procedure, 2.78 g of $FeSO_4{\cdot}7H_2O$ and 0.76 g of $NaBH_4$ were dissolved in 100 and 50 mL deoxygenated water, respectively. The resulting ferrous sulfate solution was then dropped slowly into the flask charged with $NaBH_4$ solution in 25 min under N_2 atmosphere. The flask was vigorously stirred during the addition to avoid aggregation of the resultant iron particles. The resulting black precipitates were then centrifugated, washed with water for 3 times and finally dried at 70 °C for 10 h under ambient conditions.

2.3. Characterization

The powder X-ray diffraction (XRD) pattern of the catalyst was recorded on a Scintag-XDS-2000 diffractometer with Cu Kα radiation (λ = 1.54059 Å). The size and shape of the catalyst were examined by transmission electron microscopy (TEM, Hitachi H-7500). UV–vis diffuse reflectance spectra of the samples were recorded on a UV–vis spectrophotometer (Hitachi UV-3010) with an integrating sphere attachment for their reflectance in the range of 200–800 nm and $BaSO_4$ was the reflectance standard. The X-ray photoelectron spectroscopy (XPS) data were taken on an AXIS-Ultra instrument from Kratos using monochromatic Al Kα radiation (225 W, 15 mA, 15 kV) and low-energy electron flooding for charge compensation. To compensate for surface charge effects, the binding energies were calibrated using the C_{1s} hydrocarbon peak at 284.80 eV. The concentration of hydroxyl radicals formed in the catalyst aqueous suspension was determined using a photometric method described in the literature [21,22].

2.4. Procedures and analysis

The light source was a 300-W high-pressure mercury lamp fixed inside a cylindrical Pyrex flask, which was surrounded by a circulating water jacket to cool the lamp. The exterior of the cylindrical Pyrex flask was wrapped by tinfoil, leaving just a small window (3.5 cm × 1.5 cm) at the side face. The light was then focused onto a 100 mL glass reaction vessel. The average light intensity was 15 mW/cm^2. To effectively suspend the catalyst, compressed air was bubbled from the bottom of the reactor. The reaction temperature was maintained at 25 °C.

Unless otherwise specified, 20 mg of nIOCl were dispersed in 50 mL HA solution (20 mg/L, pH 7.0). Prior to the addition of H_2O_2 (5 mM) and UVA irradiation, the suspensions were stirred in the dark for ca. 10 min for the uniform mixture. At given time intervals, 3-mL samples of the aqueous solutions were filtered through a Millipore filter (pore size 0.45 μm) to remove particles. The filtrates were analyzed by recording variations of their absorbance at 254 nm using a 752N spectrophotometer (Shanghai Precision & Scientific Instruments Co., Ltd., China). In addition, the total organic carbon (TOC) of the solution was analyzed with a Phoenix 8000 analyzer. Samples for FTIR analysis were prepared by the following procedure. The suspensions at different irradiation time were filtered to remove nIOCl particles. The solutions were evaporated by freeze-dried method. The dry residue was supported on KBr pellets. To ensure quantitative analysis, the samples were mixed with KBr at a fixed ratio (10%). The same amount of fixed powder was also used to prepare the pellets for FTIR. The infrared spectrum was recorded on a Bruker Tensor27 FTIR spectrophotometer.

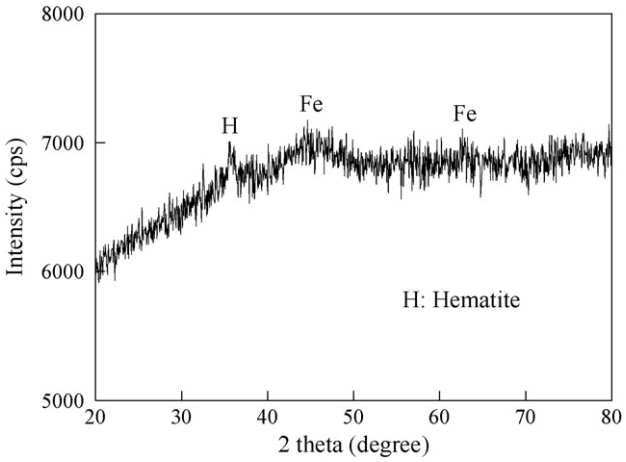

Fig. 1. XRD pattern of nIOCl.

Disinfection byproduct formation potential during the HA degradation process was assessed according to the literature [3,23]. Various HA solutions were adjusted to pH 7 with an appropriate buffer and chlorinated (30 mg/L) using concentrated NaClO solution. The chlorinated samples were then incubated at 25 °C for 72 h and extracted by 3 mL of hexane prior to DBP analysis. Trihalomethane (THM) was measured on a gas chromatograph (GC-14C, Shimadzu) equipped with OV-17 column (0.32 mm × 30 m × 0.25 μm) and an ECD detector.

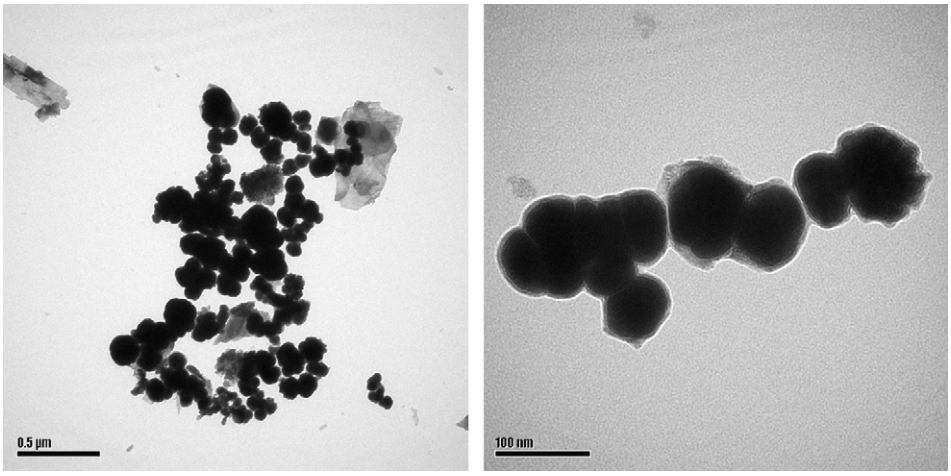

Fig. 2. TEM images of nIOCl.

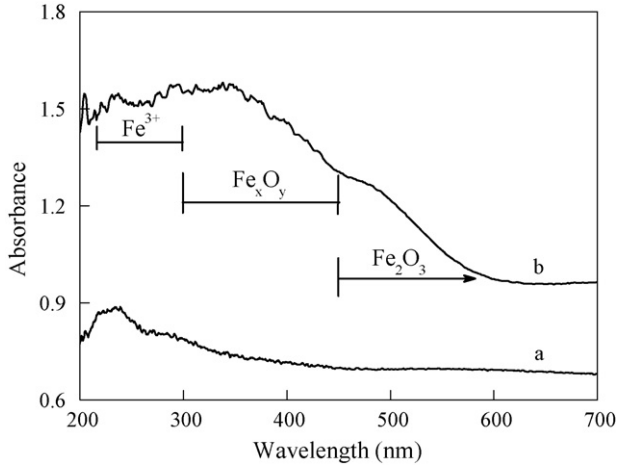

Fig. 3. UV–vis diffuse reflectance spectra of (a) Fe^0 and (b) nIOCl.

The molecular weight distribution of samples was determined by ultrafiltration [24] and the analysis was conducted using a Millipore filter (Amicon 8200) equipped with YM series membrane, having a nominal molecular weight cutoff of 30, 10 and 3 kDa. Amberlite XAD-8 and XAD-4 resins were used to determine the fractionation of HA solutions. Initial sample without pH adjustment was pumped through the XAD-8 column and the hydrophobic bases (HoB) were backflush eluted with 5 bed volumes of 0.1 mol/L H_3PO_4. While the hydrophobic neutral fraction (HoN) could not be eluted during the backflush elution process. The effluent from the XAD-8 column was acidified to pH 2 and recycled through the XAD-8 resin to enable the hydrophobic acids (HoA) to be adsorbed. The sample, which now contained weakly hydrophobic acids (WHoA) and hydrophilic matter (HiM), was then pumped through XAD-4 column and WHoA was adsorbed by XAD-4 resin. The TOC of each fraction was calculated by difference with the exception of HoB.

3. Results and discussion

3.1. Characterization of catalysts

A typical XRD pattern (Fig. 1) of the as-prepared sample matches well with the standard patterns of cubic Fe^0 (JCPDS file No. 3-1050) and Fe_2O_3 phase (Hematite, JCPDS file No. 2-915) [25]. The result showed that Fe^0 and Fe_2O_3 coexist in the as-prepared sample. As shown in Fig. 2, the prepared iron catalysts were spherical nanoparticles. The size of individual particles ranged from 50 to 100 nm, while a few particles may be as large as 200–250 nm. TEM images revealed the contrast between the gray edge and the dark center of the nanospheres, which should result from the oxidation and reaction with oxygen and water during the drying step. As shown in Fig. 3, compared with the spectrum of Fe^0 (curve a), nIOCl exhibited three absorption bands. According to the previous work [26], the first one below 300 nm was attributed to the $t_1 \rightarrow t_2$ and $t_1 \rightarrow e$ transitions of isolated Fe^{3+} ions, and the second one between 300 and 450 nm was assigned to octahedral Fe^{3+} ions in small oligonuclear clusters ($Fe_x{}^{3+}O_y$), whereas the third one above 450 nm were characteristic for larger Fe_2O_3 particles. Furthermore, the metallic state of the iron on the surface of the sample was characterized by XPS analysis. As shown in Fig. 4a, the peaks at 711, 719, and 725 eV represented the binding energies of $Fe2p_{3/2}$, shake-up satellite $Fe2p_{3/2}$, and $Fe2p_{1/2}$, respectively. No signal was detected for Fe^0 at 707 eV. These features indicated that the surface of nZVI was enclosed with a layer of iron oxide [27,28]. Since both Fe_2O_3 and FeOOH had similar features and peak positions in this region, O1s survey scan was further conducted to delineate the surface oxygen

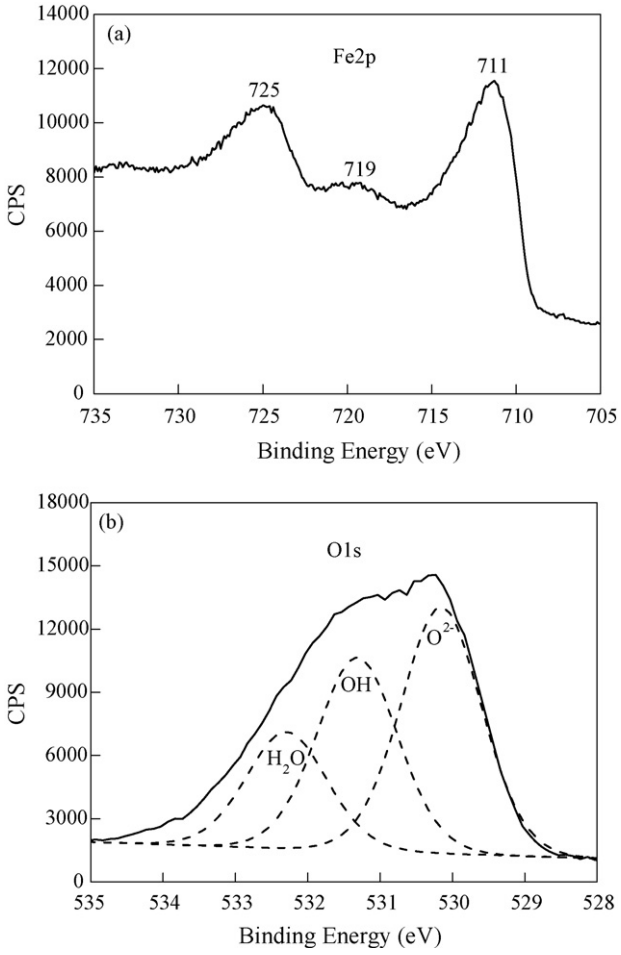

Fig. 4. XPS spectrum of nIOCl: (a) Fe2p and (b) O1s.

states. As shown in Fig. 4b, the O1s region could be decomposed into three peaks at 529.6, 531.0 and 532.2 eV, corresponding to O^{2-}, OH and chemically or physically adsorbed water [27], respectively (O^{2-}:OH:H_2O = 19.59:15.38:9.26). The existence of surface OH group suggested that FeOOH and Fe_2O_3 coexisted on the surface of nZVI.

3.2. HA degradation over nIOCl with H_2O_2 and UVA at neutral pH

The temporal absorbance changes of HA at 254 nm (A_{254}) over different iron species in the presence of H_2O_2 and UVA were shown in Fig. 5. With no catalyst, no significant HA was degraded (curve a) resulting from the direct photolysis of hydrogen peroxide under UVA irradiation at neutral pH. HA did not react with H_2O_2 over nIOCl in the dark (curve b). nZVI exhibited some activity and about 55% of HA was degraded (curve c), which could be attributed to the direct electron transfer from Fe^0 to H_2O_2 in a Haber–Weiss like mechanism. While almost complete abatement of HA was obtained within 60 min (curve d) in the presence of nIOCl under otherwise identical conditions. Only 25% degradation of HA was obtained in Fe^{3+}/H_2O_2/UVA system (curve e) even when the initial addition of Fe^{3+} in the solution was 1.4 mg/L, which was the highest concentration detected during the reaction. Therefore, the introduction of iron oxide greatly enhanced the reactivity of nZVI. Based on the redox potentials in the following equations, electron transfer process should be established at the interface of Fe^0/iron oxide. Thus, Fe^0/Fe^{2+} (Fe^0) serves as the cathode, and Fe^{2+}/Fe^{3+} (iron oxides) serves as the anode, nIOCl should have galvanic cell-like perfor-

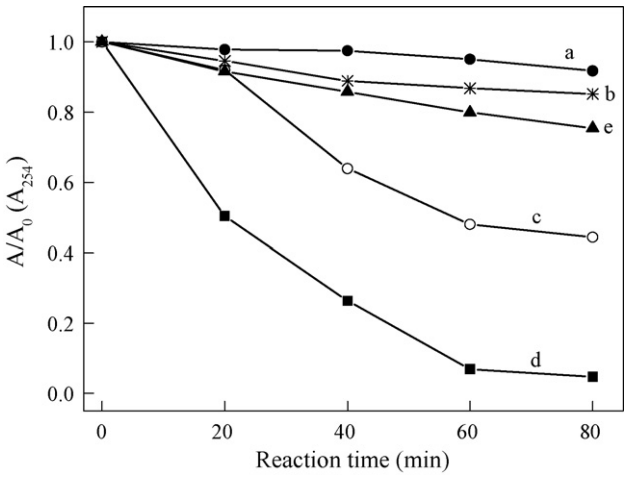

Fig. 5. Catalytic degradation of HA (50 mL, 20 mg/L) under different conditions: (a) H_2O_2 + UVA, (b) nIOCI + H_2O_2, (c) nZVI + H_2O_2 + UVA, (d) nIOCI + H_2O_2 + UVA, and (e) Fe^{3+} (1.4 mg/L) + H_2O_2 + UVA (pH 7.0, H_2O_2: 5 mM, catalyst: 0.4 g/L).

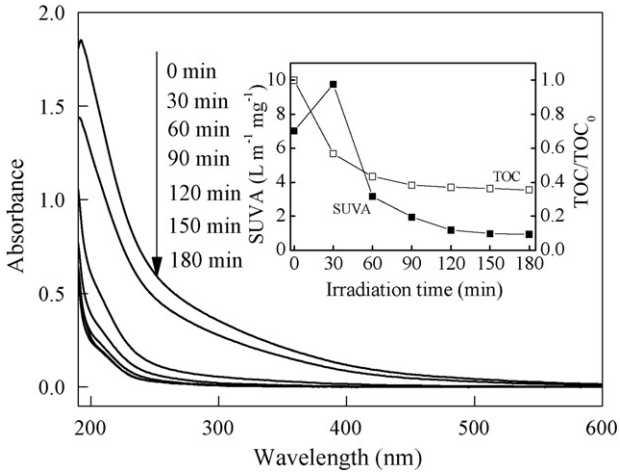

Fig. 7. UV–vis spectra, SUVA and TOC changes of HA over nIOCI in the presence of H_2O_2 and UVA (pH 7.0, H_2O_2: 5 mM, catalyst: 0.4 g/L).

mance.

$$Fe^0 - 2e^- \rightarrow Fe^{2+} \qquad E^0 = -0.440\,V \tag{1}$$

$$Fe^{3+} + 1e^- \rightarrow Fe^{2+} \qquad E^0 = 0.771\,V \tag{2}$$

$$Fe^0 + 2Fe^{3+} \rightarrow 3Fe^{2+} \qquad E^0 = 1.210\,V \tag{3}$$

To confirm this conjecture, under deoxygenated conditions in the dark, the generation of •OH was determined in aqueous nZVI and nIOCI dispersions, since under aerobic condition, the •OH could be formed by the oxidation of nZVI [29]. As shown in Fig. 6, no significant •OH formation was observed in aqueous nZVI dispersion (curve a), while the quantities of •OH increased with the reaction time (curve b) in aqueous nIOCI suspension under otherwise identical conditions. According to the published works, in the oxidative electrochemical processes, the initial step is the discharge of water molecules to form adsorbed •OH at anode surface whether O_2 exists or not [30]. The higher oxidation states on the surface of electrode are available above the thermodynamic potential from H_2O to •OH, which is lower than 1.23 V from H_2O to oxygen [31]. Therefore, the electron potential of the interface Fe^0/iron oxide, 1.21 V, is higher than that one from H_2O to •OH, resulting in that •OH radicals were produced on the surface of nIOCI in the dark under deoxygenated conditions. The result provides a solid indication that nIOCI possesses the galvanic cell-like performance.

3.3. Degradation characteristics and DBP formation of HA

As shown in Fig. 7, the absorbance values of HA solution at 254 nm decreased rapidly with the increase of irradiation time in the presence of nIOCI and H_2O_2, and there was almost no change of A_{254} observed when the heterogeneous photo-Fenton reaction proceeded 150 and 180 min. This result suggested that unsaturated components in HA might have been destroyed by the oxidation of •OH radicals during the photo-Fenton process. SUVA is defined as the UV absorbance at 254 nanometers measured in inverse meters (m^{-1}) divided by the TOC concentration measured in milligrams per liter (mg L^{-1}). Moreover, under otherwise identical conditions, SUVA reached a maximum value of 9.76 L m^{-1} mg^{-1} at 30 min and then decreased with reaction time; while 62% of the TOC content was removed after 90 min of irradiation and the TOC value was quite stable for extended periods of time (see inset, Fig. 7). The results indicated that A_{254} only yielded information on specific organic groups rather than the total dissolved organic species and the correlation between the changes of A_{254} and the TOC removal was very weak for HA solution.

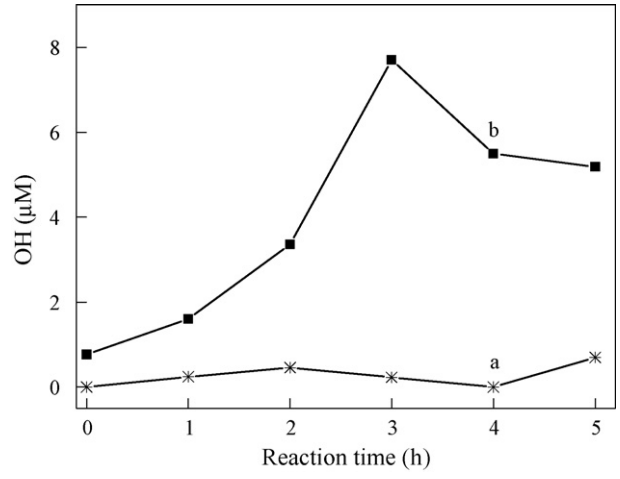

Fig. 6. Generation of hydroxyl radicals in (a) nZVI and (b) nIOCI dispersions (0.4 g/L) at pH 7.0 as a function of reaction time under deoxygenated conditions in the dark.

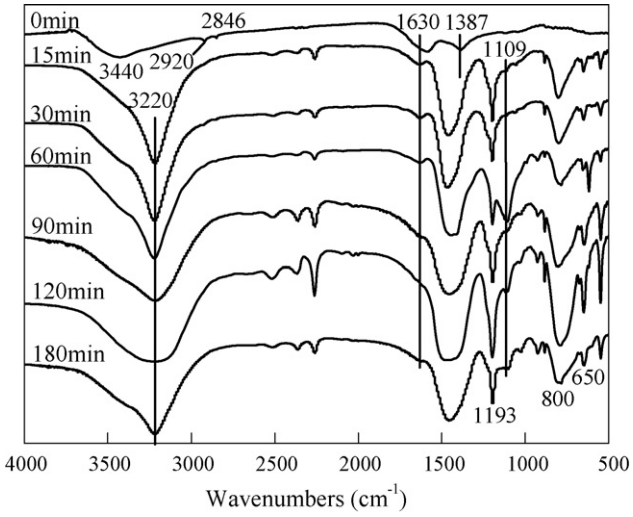

Fig. 8. Comparison of FTIR spectra between unirradiated and irradiated HA.

To further investigate the degradation process of HA and the correlation between its functional groups and the DBP formation, the FTIR spectra of HA treated for different reaction time were shown in Fig. 8. It is known that the features of the bands for the spectra of HA are at 3700–3200 cm^{-1} for phenolic O–H stretching [24] and at 2920, 2846 cm^{-1} for C–H asymmetric/symmetric stretching of $–CH_3$ and $–CH_2$ groups assigned to hydrophobic fractions [32]. Furthermore, the absorption bands at 1580–1630 cm^{-1} could be attributed to aromatic ring C=C–C and to the asymmetric C=O stretching of quinones, conjugated ketones, while the peak at 1387 cm^{-1} may be C–H stretching deformation of $–CH_3$ and $–CH_2$ groups [33], and their intensities decreased with increasing reaction times. These results suggested that the "activated" aromatic content and oxygen-rich ketones have been destroyed during the degradation process, which are generally thought to be the key factors that could enhance the reactivity of humic substances with chlorine to form DBPs [3,34]. By comparison with HA before reaction, strong O–H stretching absorption bands from 3000 to 3500 cm^{-1} are characteristic of the hydrophilic fractions [32]. On the other hand, the intensities at 1193 and at 1109 cm^{-1} corresponded to C–O the antisymmetric and symmetric stretching of ether bonds [24], appeared and then decreased with increasing irradiation time. The reasons for the decrease in peak intensity can be attributed to the formation of CO_2, which is consistent with the TOC plot in inset of Fig. 7.

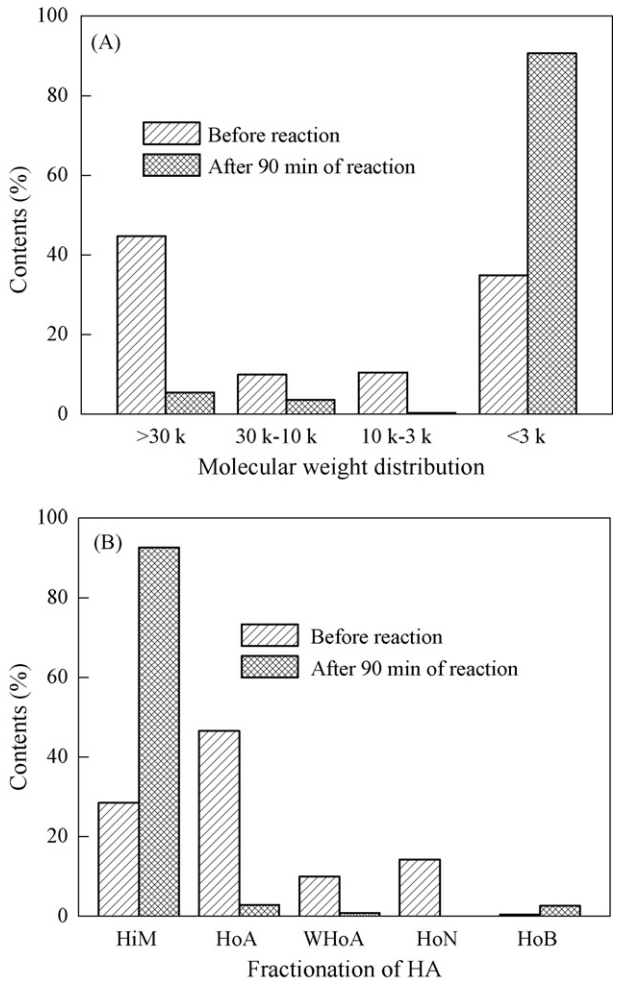

Fig. 9. The molecular and structural changes of HA before and after heterogeneous photo-Fenton degradation: (A) molecular weight distribution and (B) fractionation of HA.

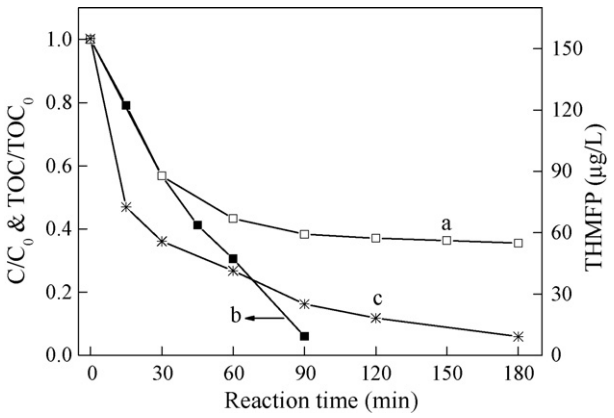

Fig. 10. Changes of TOC removal (a), H_2O_2 concentration (b) and DBPs formation (c) of HA over nIOCl in the presence of H_2O_2 and UVA (pH 7.0, H_2O_2: 5 mM, catalyst: 0.4 g/L).

Fig. 9A shows the molecular weight distribution of HA with irradiation time. Obviously, the molecular size of HA decreased rapidly with reaction time according to the reduction of the fractions of molecular weight >30, 10–30, and 3–10 kDa. The lowest molecular weight fraction (<3 kDa) was the dominant species after 90 min of reaction and the degradation of the high molecular weight fraction of HA resulted in a lowering of molecular size. The results of chemical fractional character analysis were shown in Fig. 9B, the HA solution before reaction was dominated by hydrophobic acid such that HoA > HiM > HoN > WhoA > HoB. The hydrophobic fractions (HoA, HoN, and WHoA) have greater molecular weight and aromaticity than the hydrophilic fractions and have higher reactivity toward oxidation with oxidants such as chlorine and ozone. Consequently, due to the dominance of the hydrophobic fractions, it is anticipated that the hydrophobics would account for the markedly reduction of A_{254}, TOC removal and the DBP-FPs. As expected, after 90 min of irradiation, the concentration of hydrophobics was greatly reduced, while at the same time the hydrophilic fractions increased during the heterogeneous photo-Fenton process over nIOCl.

Based on the experimental results above, it has been proven that the DBP formation was greatly correlative to the functional groups of HA such as the aromatic rings. This conjecture was further confirmed by the results shown in Fig. 10. About 62% of the TOC was removed and converted into CO_2 and H_2O after 90 min of irradiation as a result of Fenton oxidation (curve a). While the TOC value then decreased slowly when the HA solution was further irradiated for another 90 min because of the depleted H_2O_2 (curve b). However, during the degradation process, the chlorinated disinfection byproduct (THMs) formation potentials of the HA solution decreased rapidly with reaction time even when the TOC concentration reached a steady state and the decrease rate was also much higher than that of TOC removal (curve c). Although the DBP formation could be minimized significantly by reducing overall NOM concentration [3], DBP formation was rather a better indicator of HA degradation than the TOC removal.

4. Conclusion

The core–shell structure of nIOCl nanoparticles produced a highly efficient heterogeneous photo-Fenton catalyst for the degradation of humic acid. The galvanic cell-like performance of nIOCl was verified by the formation of •OH in aqueous nIOCl suspension under deoxygenated conditions in the dark. The hydrophobic fractions with higher molecular weight of HA have higher reactivity toward oxidation with oxidants and then decreased as result

of Fenton oxidation. The formation of ring-opened products and the generation of CO_2 may contribute to a decrease in molecular size of humic acid. Such changes in molecular and structural characteristics and the degradation of aromatic moieties also have a significant influence on the formation of disinfection byproducts. DBPs formation was rather a better indicator of HA degradation process.

Acknowledgments

This work was supported by the National Natural Science Foundation of China (Nos. 50778169, 50908223, 50621804, 50538090, and 20537020) and the National 863 Project of China (Grant No. 2006AA06Z304).

References

[1] T. Karanfil, J.E. Kilduff, M.A. Schlautman, W.J. Weber Jr., The oxygen sensitivity of organic macromolecule sorption by activated carbon: effects of solution chemistry, Water Res. 32 (1) (1998) 154–164.
[2] H. Katsumata, M. Sada, S. Kaneco, T. Suzuki, K. Ohta, Y. Yobiko, Humic acid degradation in aqueous solution by the photo-Fenton process, Chem. Eng. J. 137 (2) (2008) 225–230.
[3] W.J. Weber Jr., Q.G. Huang, R.A. Pinto, Reduction of disinfection byproduct formation by molecular reconfiguration of the fulvic constituents of natural background organic matter, Environ. Sci. Technol. 39 (17) (2005) 6446–6452.
[4] Y. Nagata, K. Hirai, H. Bandow, Y. Maeda, Decomposition of hydroxybenzoic and humic acids in water by ultrasonic irradiation, Environ. Sci. Technol. 30 (4) (1996) 1133–1138.
[5] A.V. Jung, V. Chanudet, J. Ghanbaja, B.S. Lartiges, J.L. Bersillon, Coagulation of humic substances and dissolved organic matter with a ferric salt: an electron energy loss spectroscopy investigation, Water Res. 39 (16) (2005) 3849–3862.
[6] D. Jermann, W. Pronk, S. Meylan, M. Boller, Interplay of different NOM fouling mechanisms during ultrafiltration for drinking water production, Water Res. 41 (5) (2007) 1713–1722.
[7] K. Okawa, Y. Nakano, W. Nishijima, M. Okada, Effects of humic substances on the decomposition of 2,4-dichlorophenol by ozone after extraction from water into acetic acid through activated carbon, Chemosphere 57 (9) (2004) 1231–1235.
[8] E.S. Mario, W. Paul, Biosorption of humic and fulvic acids to live activated sludge biomass, Water Res. 37 (10) (2003) 2301–2310.
[9] C.S. Philip, Assessing ozonation research needs in water treatment, J. Am. Water Works Assoc. 82 (10) (1990) 78–88.
[10] A.R. Radwan, J.C. David, Photocatalytic degradation of humic acid in saline waters. Part 2. Effects of various photocatalytic materials, Appl. Catal. A: Gen. 246 (1) (2003) 39–48.
[11] K. Hustert, P.N. Moza, A. Kettrup, Photochemical degradation of carboxin and oxycarboxin in the presence of humic substances and soil, Chemosphere 38 (14) (1999) 3423–3429.
[12] A.J. Motheo, L. Pinhedo, Electrochemical degradation of humic acid, Sci. Total Environ. 256 (1) (2000) 67–76.
[13] X.Z. Li, F.B. Li, C.M. Fan, Y.P. Sun, Photoelectrocatalytic degradation of humic acid in aqueous solution using a Ti/TiO_2 mesh photoelectrode, Water Res. 36 (9) (2002) 2215–2224.
[14] Z.H. Ai, L.R. Lu, J.P. Li, L.Z. Zhang, J.R. Qiu, M.H. Wu, $Fe@Fe_2O_3$ core–shell nanowires as the iron reagent. 2. An efficient and reusable sono-Fenton system working at neutral pH, J. Phys. Chem. C 111 (20) (2007) 7430–7436.
[15] I.R. Guimarães, L.C.A. Oliveira, P.F. Queiroz, T.C. Ramalho, M. Pereira, J.D. Fabris, J.D. Ardisson, Modified goethites as catalyst for oxidation of quinoline: evidence of heterogeneous Fenton process, Appl. Catal. A: Gen. 347 (1) (2008) 89–93.
[16] S.R. Kanel, J.M. Greneche, H. Choi, Arsenic(V) removal from groundwater using nano scale zero-valent iron as a colloidal reactive barrier material, Environ. Sci. Technol. 40 (6) (2006) 2045–2050.
[17] C. Noradoun, M.D. Engelmann, M. Mclaughlin, R. Hutcheson, K. Breen, A. Paszczynski, I.F. Cheng, Destruction of chlorinated phenols by dioxygen activation under aqueous room temperature and pressure conditions, Ind. Eng. Chem. Res. 42 (21) (2003) 5024–5030.
[18] F.C.C. Moura, M.H. Araujo, R.C.C. Costa, J.D. Fabris, J.D. Ardisson, W.A.A. Macedo, R.M. Lago, Efficient use of Fe metal as an electron transfer agent in a heterogeneous Fenton system based on Fe^0/Fe_3O_4 composites, Chemosphere 60 (8) (2005) 1118–1123.
[19] R.C.C. Costa, F.C.C. Moura, J.D. Ardisson, J.D. Fabris, R.M. Lago, Highly active heterogeneous Fenton-like systems based on Fe^0/Fe_3O_4 composites prepared by controlled reduction of iron oxides, Appl. Catal. B: Environ. 83 (1–2) (2006) 131–139.
[20] A. Georgi, A. Schierz, U. Trommler, C.P. Horwitz, T.J. Collins, F.D. Kopinke, Humic acid modified Fenton reagent for enhancement of the working pH range, Appl. Catal. B: Environ. 72 (1–2) (2006) 26–36.
[21] C.F. Babbs, M.J. Gale, Colorimetric assay for methanesulfinic acid in biological samples, Anal. Biochem. 163 (1987) 67–73.
[22] M.G. Steiner, C.F. Babbs, Quantitation of the hydroxyl radical by reaction with dimethyl sulfoxide, Arch. Biochem. Biophys. 278 (2) (1990) 478–481.
[23] B. Kwon, S. Lee, J. Cho, H. Ahn, D. Lee, H.S. Shin, Biodegradability, DBP formation, and membrane fouling potential of natural organic matter: characterization and controllability, Environ. Sci. Technol. 39 (3) (2005) 732–739.
[24] M. Fukushima, K. Tatsumi, Degradation characteristics of humic acid during photo-Fenton processes, Environ. Sci. Technol. 35 (18) (2001) 3683–3690.
[25] Z.H. Ai, L.R. Lu, J.P. Li, L.Z. Zhang, J.R. Qiu, M.H. Wu, $Fe@Fe_2O_3$ core–shell nanowires as iron reagent. 1. Efficient degradation of rhodamine B by a novel sono-Fenton process, J. Phys. Chem. C 111 (11) (2007) 4087–4093.
[26] J. Perez-Ramirez, M.S. Kumar, A. Bruckner, Reduction of N_2O with CO over FeMFI zeolites: influence of the preparation method on the iron species and catalytic behavior, J. Catal. 223 (1) (2004) 13–27.
[27] X.Q. Li, W.X. Zhang, Iron nanoparticles: the core–shell structure and unique properties for Ni (II) sequestration, Langmuir 22 (10) (2006) 4638–4642.
[28] A.P. Grosvenor, B.A. Kobe, M.C. Biesinger, N.S. Mclntyre, Investigation of multiplet splitting of Fe 2p XPS spectra and bonding in iron compounds, Surf. Interface Anal. 36 (12) (2004) 1564–1574.
[29] S.H. Joo, A.J. Feitz, D.L. Sedlak, T.D. Waite, Quantification of the oxidizing capacity of nanoparticulate zero-valent iron, Environ. Sci. Technol. 39 (5) (2005) 1263–1268.
[30] B. Marselli, J. Garcia-Gomez, P.A. Michaud, M.A. Rodrigo, Ch. Comninellis, Electrogeneration of hydroxyl radicals on boron-doped diamond electrodes, J. Electrochem. Soc. 150 (3) (2003) D79–D83.
[31] R.S. Juang, S.W. Wang, Electrolytic recovery of binary metals and EDTA from strong complexed solutions, Water Res. 34 (12) (2000) 3179–3185.
[32] J.A. Leenheer, Comprehensive approach to preparative isolation and fractionation of dissolved organic carbon from natural waters and wastewaters, Environ. Sci. Technol. 15 (5) (1981) 578–587.
[33] B.H. Gu, J. Schmitt, Z.H. Chen, L.Y. Liang, J.F. McCarthy, Adsorption and desorption of natural organic matter on iron oxide: mechanisms and models, Environ. Sci. Technol. 28 (1) (1994) 38–46.
[34] D.L. Norwood, J.D. Johnson, R.F. Christman, J.R. Hass, M.J. Bobenrieth, Reactions of chlorine with selected aromatic models of aquatic humic material, Environ. Sci. Technol. 14 (2) (1980) 187–190.